Computational Low-Frequency Electromagnetic Dosimetry Based on Magnetic Field Measurements

Computational low frequency electromagnetic dosimetry based on magnetic field measurements

Authors

Alessandro Arduino[a]*, Oriano Bottauscio[a], Mario Chiampi[a], Ilkka Laakso[b], Luca Zilberti[a]

Author affiliation

[a] Istituto Nazionale di Ricerca Metrologica (INRIM) – 10135 Torino, Italia

[b] Department of Electrical Engineering and Automation – Aalto University – Espoo, Finland

* Correspondence should be addressed to: a.arduino@inrim.it

Published journal article available at DOI: https://doi.org/10.1109/JERM.2018.2869021

Computational Low Frequency Electromagnetic Dosimetry Based on Magnetic Field Measurements

Alessandro Arduino, Oriano Bottauscio, Mario Chiampi, Ilkka Laakso, and Luca Zilberti

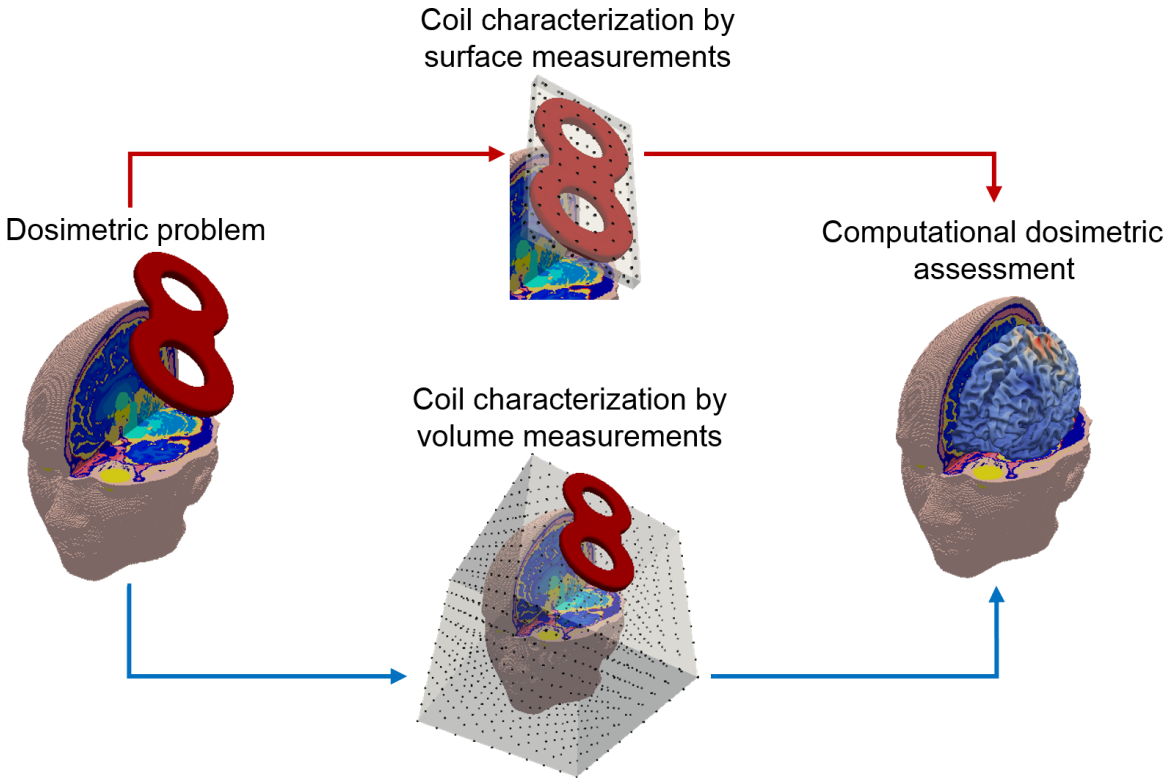

Scheme of the experimental-computational techniques discussed in this paper.

Take-Home Messages

- We propose an experimental-computational technique for low frequency dosimetric assessments that reduces the experimental burden while maintaining accuracy and robustness.
- The proposed technique can be used when the magnetic source is unknown or not suitable to be modeled.
- By adopting surface measurements, the proposed technique allows to characterize any low frequency magnetic source in a very convenient way.
- By adopting the boundary element method for extrapolating surface measurements as well as a curl inversion operator for magnetic vector potential evaluation, the proposed technique significantly reduces the noise from the input data.
- The positive features of the proposed technique have been put in evidence by testing it in a transcranial magnetic stimulation dosimetric application.

Computational Low Frequency Electromagnetic Dosimetry Based on Magnetic Field Measurements

Alessandro Arduino, Oriano Bottauscio, Mario Chiampi, Ilkka Laakso, and Luca Zilberti

Abstract This paper compares different experimental-computational strategies for the estimation of electric fields induced in human bodies by low frequency magnetic sources characterized by a set of magnetic field measurements. The analysis is carried out by considering three alternative procedures, which use, as the first input, the distribution of the magnetic flux density in a volume containing the studied body or on a surface surrounding the sources. The comparison is performed on a realistic model problem, related to transcranial magnetic stimulation (TMS), in which numerically simulated "virtual measurements" are employed. The comparative analysis is developed in terms of both result accuracy and robustness against noisy input due to unavoidable experimental uncertainties. It results that by performing the measurements on a surface surrounding the sources, a significant reduction of the experimental burden is found with respect to the case of volume measurements, without affecting neither the accuracy nor the robustness of the procedure. In particular, when whole body electric field evaluation must be carried out, the advantage of surface measurements with respect to volume ones becomes significant. Moreover, a preferable scheme obtained as hybridization of previously proposed strategies is identified. Besides the adoption of a TMS model problem in the comparison procedure, the achieved result can be extended to any low frequency dosimetric assessment where the magnetic sources are difficult to model or not completely known.

Keywords **— Biomedical computing, Dosimetry, Electromagnetic fields, Numerical analysis, Uncertainty.**

I. Introduction

QUANTITAVE evaluation of the electric phenomena induced in human bodies by low frequency (LF) magnetic fields (up to 1 MHz) is a problem of large interest not only in occupational or residential environments, but also in the medical sector, due to the increasing application of electromagnetic devices for diagnostic and therapeutic purposes, like in transcranial magnetic stimulation (TMS). Apart from measurements in liquid phantoms, the exposure is estimated by solving, analytically or numerically, an electromagnetic field problem, starting from a description of the magnetic sources. However, this approach cannot be applied when the sources are unknown or only partially known (e.g., not well specified by the device builder), or difficult to be modelled (e.g., with too many elements, as in electrical substations, or in presence of active or passive thin shields). In such cases, only measurements of the magnetic flux density in a limited number of points can be used to characterize the sources. Then, the measured data can be elaborated by following two distinct approaches. The first one uses the measurements to identify equivalent sources able to reproduce with reasonable accuracy the magnetic field distribution [1]-[5]. The exposure is then evaluated by applying the classical analytical or numerical methods. The other approach, which is investigated in this paper, develops a specific electromagnetic field formulation in which the experimental data are employed as input for the electromagnetic problem. In this case, the magnetic flux density can be either; (a) directly measured in the volume that will be occupied by the biological tissues [6], [7], or (b) measured on a surface surrounding the source without including any portion of the radiated body [8], [9]. When volume measurements are performed, the experimental burden is usually reduced through interpolation and extrapolation techniques. In case of surface measurements, additional computations are required in order to obtain the distribution of the magnetic field inside the body.

This paper analyzes advantages and drawbacks of three strategies. In one case, volume measurements are elaborated by a *curl* inversion formula [6], [10], [11] to evaluate the magnetic vector potential $\boldsymbol{A}$ used as forcing term in an electromagnetic field formulation based on $\boldsymbol{A}$

Manuscript received XXX XX, XXXX; revised XXX XX, XXXX; accepted XXX XX, XXXX. Date of pubblication XXX XX, XXXX; date of current version XXX XX, XXXX. *(Corresponding author: Alessandro Arduino.)*

A. Arduino, O. Bottauscio, M. Chiampi and L. Zilberti are with the Division of Metrology for Quality of Life, Istituto Nazionale di Ricerca Metrologica, 10135 Torino, Italy (e-mail: a.arduino@inrim.it; o.bottauscio@inrim.it; m.chiampi@inrim.it; l.zilberti@inrim.it).

I. Laakso is with the Department of Electrical Engineering and Automation, Aalto University, Espoo, Finland (e-mail: ilkka.laakso@aalto.fi).

Color versions of one or more of the figures in this paper are available online at http://ieeexplorer.iee.org.

Digital Object Identifier XXX

and on the electric scalar potential φ. In the second case, surface measurements performed around the source are elaborated through a Boundary Element Method (BEM) [8], [9] to get the magnetic flux density in the computational domain, which is used as forcing term of an electric vector potential $\boldsymbol{T}$ formulation. Finally, a hybridization of the two procedures, that elaborates the surface measurements with BEM and obtains $\boldsymbol{A}$ via *curl* inversion, is proposed and analyzed. These strategies for LF dosimetry have been chosen because their integral treatment of measured data ensures robustness of the procedure against the unavoidable random measurement uncertainty.

After a description of the considered experimental-computational techniques in section II, section III analyzes them in a TMS application, whose interest is increasing due to its capability of non-invasively activating or disrupting brain functions for both diagnostic and therapeutic purposes. TMS is a convenient and useful test bench, because often the features of the electric circuits inside the stimulator are not available or the source modelling is made very complicated by the addition of passive and active elements for increasing the focality [12]-[17] or protecting the operators [18]-[20]. Lastly, in section IV, the investigation is extended to the evaluation of the uncertainties in the induced electric field estimate due to the unavoidable measurement errors, which are propagated through the computational procedure.

II. Methods and Procedures

The dosimetry problem to be solved consists in computing the electric field generated in a human body, or in a portion of it, by a magnetic source that cannot be modelled (because it is unknown or too complex to be accurately described). The source is assumed to operate under LF sinusoidal conditions with angular frequency ω, so that the problem can be formulated in the frequency domain using phasors (with $\exp(j\omega t)$ convention, being j the imaginary unit) to represent the field quantities. The biological tissues are assumed magnetically neutral with constant vacuum permeability and the displacement currents are neglected. In addition, the electric conductivity is considered to be sufficiently small so that the induced currents cannot modify the magnetic field impressed by the source at the analyzed frequencies. Both assumptions comply with the actual properties of the human tissues at LF [21], [22]. To deal with this problem, volume and surface mappings of the magnetic flux density are used as input data.

The experimental-computational techniques studied in this paper are sketched in the flowchart of Fig. 1, where the boxes represent data and the arrows denote the operations. Two starting experimental datasets can be distinguished: the magnetic flux density $\boldsymbol{B}$ measured on a surface S surrounding the sources and possible additional components (e.g., shields), or $\boldsymbol{B}$ values detected within a volume V. The region Ω that will be occupied by the body must be included in volume V, without intersecting surface S. The measurement results are elaborated through numerical techniques to evaluate the distribution of the electric field $\boldsymbol{E}$ (i.e., the dosimetric quantity) inside the body Ω. The three computational schemes, here applied to process the starting experimental data, are identified in Fig. 1 by the arrow colors.

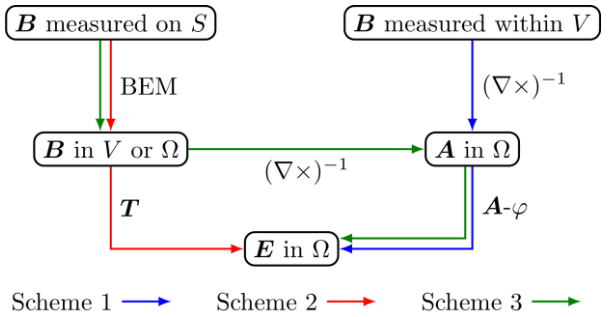

Fig. 1. Flowchart of the experimental-computational techniques discussed in this paper. The boxes represent data and the arrows indicate operations to elaborate them. The symbol $(\nabla\times)^{-1}$ denotes the *curl* inversion. The arrow colors blue, red, and green indicate the schemes 1, 2, and 3, respectively.

Scheme 1, denoted by blue arrows in Fig. 1, uses the *curl* inversion formula proposed in [6] to transform the $\boldsymbol{B}$ values measured within the volume V in the magnetic vector potential $\boldsymbol{A}$ evaluated inside the region Ω. It is worth noting that the number of points in which $\boldsymbol{A}$ is computed is, in general, much larger than the number of measurement points, since the discretization of Ω is finer than that of V. Then, the solution of an electromagnetic field problem with an $\boldsymbol{A}$-φ formulation [22] provides the electric field distribution in Ω by using the potential $\boldsymbol{A}$ as forcing term.

Scheme 2, denoted by red arrows in Fig. 1, starts from measurements of $\boldsymbol{B}$ on S and obtains the magnetic flux density distribution inside Ω following a BEM approach [23]. The result becomes the input of an electromagnetic field problem with $\boldsymbol{T}$ formulation to provide the dosimetric quantity. It is worth pointing out that, thanks to the BEM approach, surface measurements can be used for determining the field in any point of free-space, whereas the volume measurements used in scheme 1 identify a limited region in which the computational domain must be located.

Lastly, scheme 3, denoted by green arrows in Fig. 1, combines the previous techniques by starting from surface measurements, extrapolating the magnetic flux density values within the volume V by BEM and applying *curl* inversion to obtain the magnetic vector potential in Ω. At last, the $\boldsymbol{A}$-φ formulation gives the electric field values.

It is worth noting that the two considered electromagnetic formulations (i.e., $\boldsymbol{T}$ and $\boldsymbol{A}$-φ) are complementary. Thus, their numerical discretizations by a finite element method (FEM), despite converging to the same electromagnetic solution, lead intrinsically to different numerical approximations [24], [25]. This fact must be taken into account in order to correctly evaluate the accuracy of the experimental-computational techniques.

A. *Curl inversion formula*

Different techniques have been proposed in literature in order to perform *curl* inversion. The formula suggested in [6] have been adopted in this paper because of its attractive features with respect to other strategies [10], [11], which require the knowledge of $\boldsymbol{B}$ everywhere in space or imply a greater numerical effort. Thus, the vector potential $\boldsymbol{A}$ is obtained by integrating $\boldsymbol{B}$ in accordance to the following relation, whose numerical implementation on Cartesian grids is extremely efficient. For any index $i \in \{1, 2, 3\}$,

$$A_i(\boldsymbol{x}) = \sum_{j,k=1}^{3} \varepsilon_{ijk} \int_0^{x_k} \left(\frac{1}{3} B_j(\boldsymbol{x}) + \frac{1}{6} B_j\left(\boldsymbol{x}_0^j\right) \right) \mathrm{d}x_k , \qquad (1)$$

where $\boldsymbol{x} = (x_1, x_2, x_3)$ are the spatial coordinates, ε_{ijk} is the Levi-Civita symbol, and $\boldsymbol{x}_0^j = ((1-\delta_{1j})x_1, (1-\delta_{2j})x_2, (1-\delta_{3j})x_3)$ with δ_{ij} the Kronecker delta.

The described potential $\boldsymbol{A}$ can be evaluated numerically in any point, but not all its analytical properties can be stated. For example, the value of its divergence depends on the choice of the origin of the reference system. In addition, such a value in general changes from point to point, hindering an explicit analytical expression for it.

B. *Boundary element method*

In order to extrapolate the data measured on the surface S surrounding the magnetic sources in points belonging to a volume (Ω or V), BEM is employed [23]. To do that, surface S is discretized into M mesh elements (S_m for $m = 1, \ldots, M$) in whose barycenters $\boldsymbol{B}$ is measured. The magnetic flux density is assumed uniformly distributed in each mesh element, so the following relation provides the value of $\boldsymbol{B}$ in any point P outside S,

$$\boldsymbol{B}(P) = \sum_{m=1}^{M} (\boldsymbol{n} \times \boldsymbol{B})_m \times \int_{S_m} \nabla \Psi_{P,m} \, dS + \sum_{m=1}^{M} (\boldsymbol{n} \cdot \boldsymbol{B})_m \int_{S_m} \nabla \Psi_{P,m} \, dS \qquad (2)$$

where $\boldsymbol{n}$ is the normal unit vector directed outwards from S, subscript m denotes evaluation in S_m barycenter and $\Psi_{P,m} = 1/(4\pi r_{P,m})$ is the Green's function, being $r_{P,m}$ the distance between the computation point P and the source point (i.e., the integration point in S_m).

The implementation of BEM is more expensive than simple *curl*-inversion, but anyway its computational cost is small with respect to the solution of the electromagnetic field problem.

C. $\boldsymbol{A}$-φ *formulation*

Once the magnetic vector potential $\boldsymbol{A}$ is known in Ω, the electric scalar potential φ can be computed by solving

$$\begin{cases} \nabla \cdot (\sigma \nabla \varphi) = \mathrm{j}\omega \nabla \cdot (\sigma \boldsymbol{A}), & \text{in } \Omega \\ \boldsymbol{n} \cdot \nabla \varphi = \mathrm{j}\omega \boldsymbol{n} \cdot \boldsymbol{A}, & \text{on } \partial\Omega \end{cases} \qquad (3)$$

where σ is the electric conductivity of the biological tissues and $\boldsymbol{n}$ is the outward unit vector. The electric field is then obtained as $\boldsymbol{E} = -\nabla\varphi + \mathrm{j}\omega\boldsymbol{A}$.

Here, equation (3) is numerically solved using FEM with first-order cubical elements. The linear equation system can be solved using the matrix-free geometric multigrid method with successive over relaxation [26] or the GMRES algorithm [27]. The application of the $\boldsymbol{A}$-φ formulation requires necessarily the additional operation of the *curl* inversion, because the vector potential cannot be directly measured. However, the related field problem, which uses as unknowns the nodal values of a scalar quantity, has a limited size and can usually be solved efficiently.

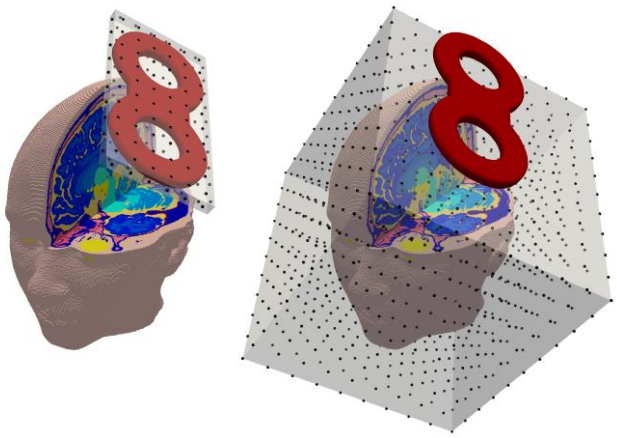

Fig. 2. Head and TMS device models with possible measurement points.

D. $\boldsymbol{T}$ *formulation*

By expressing the current density distribution $\boldsymbol{J} = \sigma\boldsymbol{E}$ induced in the body Ω through an electric vector potential $\boldsymbol{T}$ (i.e., $\boldsymbol{J} = \nabla \times \boldsymbol{T}$), the field problem becomes

$$\begin{cases} \nabla \times \left(\frac{1}{\sigma} \nabla \times \boldsymbol{T} \right) = -\mathrm{j}\omega \boldsymbol{B}, & \text{in } \Omega \\ \boldsymbol{T} \times \boldsymbol{n} = \boldsymbol{0}, & \text{on } \partial\Omega \end{cases} \qquad (4)$$

where $\boldsymbol{n}$ is the outward unit vector. The problem is solved by FEM using the cubic voxels that discretize Ω as edge elements [28]. The formulation is kept ungauged and the related indeterminate linear system is solved by the GMRES algorithm [27].

The $\boldsymbol{T}$ formulation is directly driven by $\boldsymbol{B}$ values, but the number of unknowns defined on the voxel edges is about threefold of nodal quantities and hence the processing time increases significantly.

III. Results

A. *Application to TMS device*

The analysis of the electric field generated in the head of a patient during a TMS session is used as a test bench for the comparison of the three schemes. This model problem is realistic because, in TMS treatment planning, an accurate knowledge of the effect produced by the LF magnetic sources is required, but, often, the design of the coil is unknown or too complicated to be modeled. A figure-of-eight TMS coil with sinusoidal supply at 1 kHz is arranged near the patient head, as depicted in Fig. 2.

The patient head (i.e., the computational volume Ω) is modelled by an anatomical model [29] truncated at the neck and divided into 1 mm side cubic voxels, which are used as finite elements in the numerical procedures. The model includes 35 biological tissues whose electric conductivities

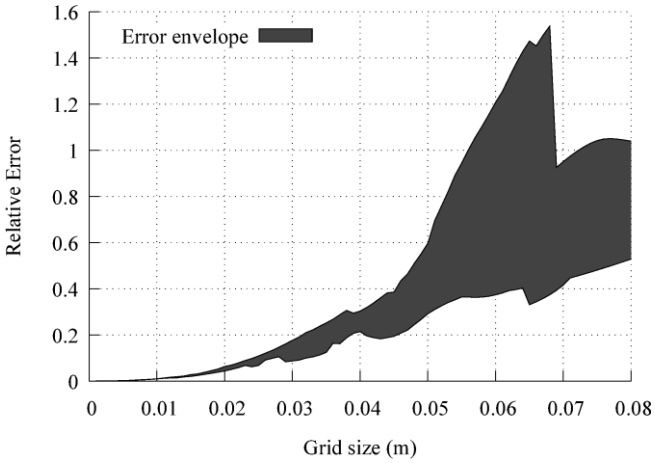

Fig. 3. Relative error Δ versus measurement grid size in scheme 1. The black area defines the envelope of the results for 20 positioning of volume V for each grid size.

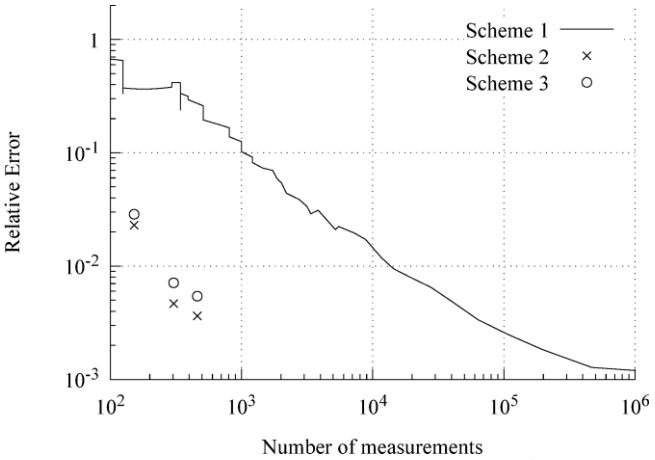

Fig. 4. Relative error Δ versus measurement number for the three considered schemes.

are assumed according to the values adopted in [6].

The TMS coil is modelled by circular line sources with known currents. The magnetic flux density or vector potential generated by the coil are computed in any spatial point by the Biot–Savart law, which is used as a "mathematical probe" for the virtual measurements.

The analysis of the techniques is performed evaluating the global error committed in the recovery of the electric field in the head starting from virtual measurements. The relative error Δ is defined by

$$\Delta = \sqrt{\sum_{k=1}^{K} \left| \boldsymbol{E}_k^0 - \boldsymbol{E}_k \right|^2 \Big/ \sum_{k=1}^{K} \left| \boldsymbol{E}_k^0 \right|^2} \qquad (5)$$

where K is the number of employed voxels, $\boldsymbol{E}_k$ is the value of the electric field in the barycenter of the k-th voxel of the head computed by applying the experimental-computational technique, whereas $\boldsymbol{E}_k^0$ is the corresponding value of the reference field. To compute the reference field, the Biot–Savart law is employed to directly provide the forcing term of the electromagnetic problem in each voxel. It is worth noting that, because of the complementarity of the used formulations [24], [25], each formulation must adopt its specific reference field in order to avoid an intrinsic bias, which could alter the evaluation of the performances.

Scheme 1 is applied to virtual measurements performed within a volume V, which is a parallelepiped aligned with the plane of the TMS coil. Volume V contains the entire head model Ω without intersecting any part of the source. V is discretized in accordance to a Cartesian grid at whose nodes the magnetic flux density is measured. To test the effect of grid positioning, the center gridline of V is shifted from the center of the TMS coil by $(sr_u\boldsymbol{u} + sr_v\boldsymbol{v})$, where s is the grid size, $\boldsymbol{u}$ and $\boldsymbol{v}$ are the directions of the main axes of volume V in the plane of the TMS coil, and r_u and r_v are random numbers extracted in [-0.5, 0.5] from a uniform probability distribution. The *curl* inversion formula appears to be sensitive to the choice of the grid size and of the positioning of the volume V itself, as can be deduced from Fig. 3. In this figure, the envelope of the global error Δ committed by the scheme is reported as a function of the grid size ranging from 8 cm (128 measurement points) to 1 mm (~$13.8 \cdot 10^6$ measurement points), taking into account 20 different positions of the gridlines of volume V for each resolution.

As expected, the relative error and the amplitude of the envelope decrease when reducing the grid size. For grid sizes below about 2 cm, all curves of Δ nearly coincide and the relative error is less than 10 %. The small number of random extractions for the positioning justifies the presence of discontinuities in the envelope of the global error Δ.

The surface measurements are performed on the six faces of the 21 cm × 10 cm × 1 cm parallelepiped which surrounds the TMS coil without including any portion of the human head depicted in Fig. 2. Each face is discretized into rectangular elements, making use of three meshes: 10×6×1 elements (152 measurement points), 16×8×1 elements (304 measurement points), and 20×10×1 elements (460 measurement points). The relative errors Δ as a function of number of measuring points are presented in Fig. 4 for the three adopted schemes. The procedures that start from surface measurements (i.e., schemes 2 and 3) are much more efficient than scheme 1: the global relative error is reduced by about one order of magnitude when the same number of measurement points is employed. In order to reach the same accuracy as schemes 2 and 3, scheme 1 requires the measurement in a number of points between 3000 and 20000. Scheme 2 is a little more accurate than scheme 3, but the related $\boldsymbol{T}$ formulation requires processing times significantly higher than the $\boldsymbol{A}$-φ formulation, also taking into account that scheme 3 needs the additional operation of *curl* inversion. Overall, scheme 3 seems the best trade-off between experimental and computational burdens when noise-free measurements are used.

B. Measurement uncertainty and its propagation

In a real application, the proposed schemes would suffer from the unavoidable measurement uncertainty. Thus, it is necessary to verify the robustness of the procedures against the random variability of the input data. Uncertainty propagation has already been investigated for scheme 1 in [6], where the noise filtering effect of *curl* inversion has

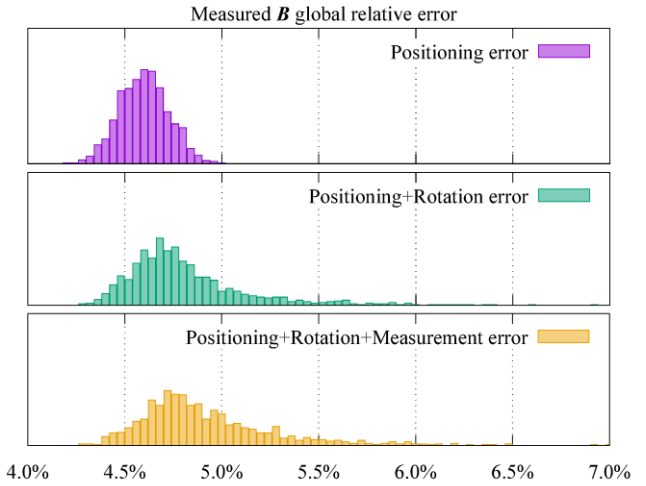

Fig. 5. Relative frequency histograms of the global relative error in virtual measurements of the magnetic flux density on the surface S, computed in analogy to (5). Incremental contributions to the error due to misplacement and misalignment of the probe and instrumental uncertainty are collected. The intermediate mesh, with 304 surface measurements, has been used.

been put in evidence. In this paper, the analysis is extended to schemes 2 and 3, which have been found to be the most advantageous approaches.

The random error in the virtual measurement data, used to perform the robustness analysis, is modelled by considering three contributions to the uncertainty: (*a*) displacement of the probe with respect to the chosen position, (*b*) rotation of the probe with respect to a local coordinate system centered on the measurement point, and (*c*) instrumental uncertainty. The positioning error along each Cartesian axis is extracted from an isosceles trapezoidal distribution within -1 mm and 1 mm, with uniform region from -0.5 mm to 0.5 mm, which models a completely unknown positioning in the uniform region and a less probable occurrence of wider displacements [30]. A rotation axis and an amplitude of rotation are used to describe the rotation error. A unit vector extracted from a uniform distribution on the sphere identifies the rotation axis [31]—no preferential direction is chosen—, whereas the amplitude is modelled by a normal distribution with null mean and standard deviation equal to 1°, so that big errors are possible but about 99.73 % of the times the amplitude is less than 3° [30]. The rotation error is attributed to a flawed positioning of the probe when it is assembled on the measuring system, so the error is kept constant in all measurement points. Lastly, the instrumental uncertainty includes a calibration factor and a background stray field. A normal distribution with null mean and standard deviation equal to 1 % models the uncertainty in the calibration factor, which is kept constant in all measurement points being a systematic error. Each component of the background stray field is extracted according to a uniform distribution between -3 nT and 3 nT in each measurement point. Actually, this contribution, chosen by assuming measurements performed under controlled laboratory conditions, is negligible because of the intensity of the magnetic flux density near a TMS coil. The distributions

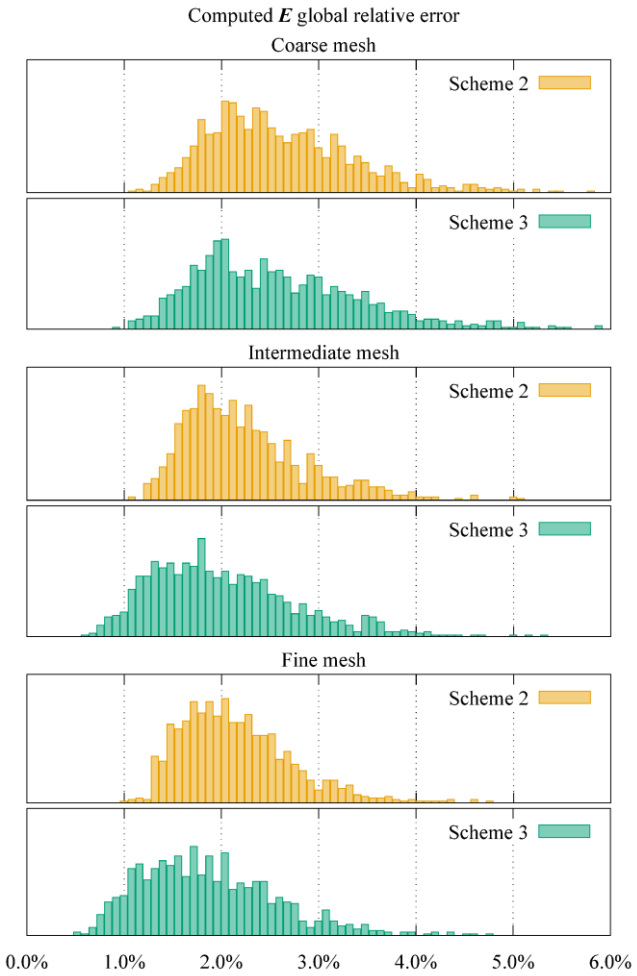

Fig. 6. Relative frequency histograms of the global relative error (5) in the dosimetric quantity retrieved in Ω by schemes 2 and 3. The error distributions are reported for each of the surface meshes used to provide the virtual measurements.

modelling the instrumental uncertainty derives from previous experience on magnetic field measurements [32].

The distribution of the resulting global relative error in the input data, defined in analogy to (5), is reported for a particular case in Fig. 5, where the incremental contribution to the error due to misplacement and misalignment of the probe and instrumental uncertainty are also presented. It can be noted that the main source of uncertainty is the positioning error, which leads to a Gaussian-like distribution of the global relative error centred at about 4.6 %. The addition of the rotation error extends the right tail of the distribution, breaking its symmetry and increasing the expected global error to about 4.8 %. Instrumental uncertainty alters the distribution negligibly.

Figure 6 collects the distributions of global relative errors Δ estimated by means of 1000 extractions of the random error of the input virtual measurements, in accordance to a Monte Carlo method. All the achieved distributions put in evidence the reduction of global error from the input (Fig. 5) to the ultimate dosimetric quantity (Fig. 6). The regularization effect is motivated by the presence of integral operators in the experimental-

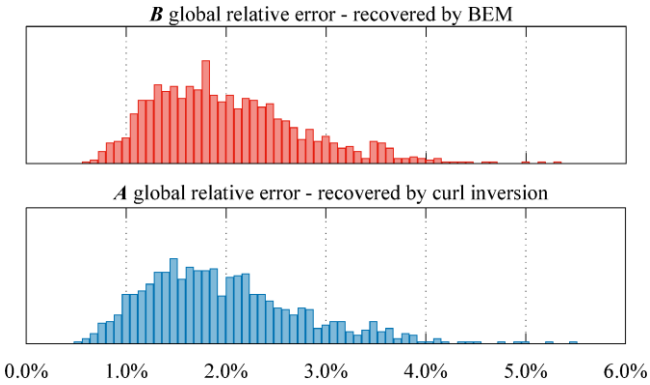

Fig. 7. Relative frequency histograms of the global relative error in intermediate steps of the experimental-computational techniques, computed in analogy to (5). The intermediate mesh, with 304 surface measurements, has been used.

TABLE I
MEAN AND STANDARD DEVIATION OF THE DISTRIBUTIONS OF ERROR IN THE RECOVERED ELECTRIC FIELD REPORTED IN FIG. 6

Scheme	Surface mesh	Mean	Standard Deviation
2	Coarse	2.61 %	0.65 %
3	Coarse	2.57 %	0.84 %
2	Intermediate	2.24 %	0.63 %
3	Intermediate	2.01 %	0.75 %
2	Fine	2.15 %	0.57 %
3	Fine	1.86 %	0.69 %

computational techniques (BEM for both schemes 2 and 3, and also *curl* inversion for scheme 3), which act as noise filters. This behavior is depicted in Fig. 7, where the distributions of the global errors in the intermediate data used by the schemes show a translation towards zero with respect to the distribution of Fig. 5.

As expected, the adoption of finer surface meshes leads to results with lower global relative errors, as confirmed by Fig. 6 and Table I. This fact is more evident when comparing the coarse mesh with the intermediate one, whereas it is slightly present between the intermediate and the fine meshes. Moreover, scheme 3 provides an additional improvement with respect to scheme 2, which becomes clear when finer meshes are considered. Anyway, the reduction of the mean global error from scheme 2 to scheme 3 comes together with the enlargement of its distribution, as can be seen also from the standard deviation collected in Table I.

Finally, the contribution of the different uncertainty sources on the dosimetric quantity is investigated. The result is reported in Fig. 8. It can be noted that, differently from the magnetic flux density (Fig. 5), the distribution of the error in the electric field due only to measurement misplacements is not symmetric. However, as well as in Fig. 5, the addition of a rotation error increases the right tail of the distribution. More precisely, the mean value of the distribution moves from 1.35 % to 1.78 % when the rotation error is added, and the standard deviation increases from 0.40 % to 0.68 %. A significant further increase is produced by the instrumental uncertainty, as can be deduced from

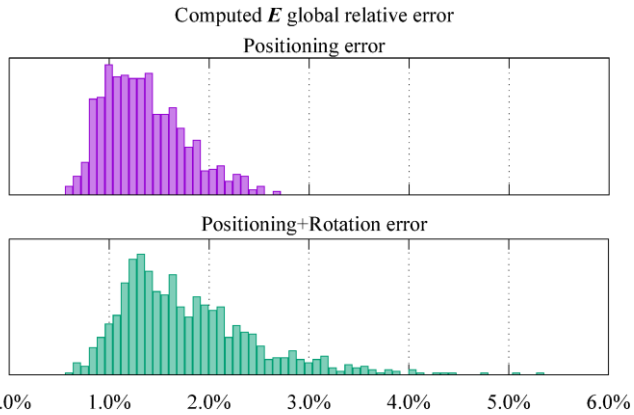

Fig. 8. Relative frequency histogram of the global relative error (5) in the dosimetric quantity retrieved in Ω by scheme 3 with input data provided on the intermediate mesh with incremental contributions to the error due to misplacement and misalignment of the probe. To be compared with Fig. 6, where all the uncertainty sources are considered.

Table I. It is worth noting that, despite the instrumental uncertainty introduces a globally negligible effect to the magnetic flux density measurement, it affects significantly the estimation of the dosimetric quantity, almost as much as the error due to probe misalignment. This is probably due to the systematic nature of the error in the calibration factor, which affects the magnetic flux density recovered by BEM. Indeed, the mean value of the global relative error in recovered $\boldsymbol{B}$ is equal to 1.16 %, 1.58 %, and 1.84%, respectively, by introducing the sources incrementally.

IV. CONCLUSION

The analysis of three experimental-computational techniques for dosimetric assessment in presence of unknown (or complicated) low-frequency magnetic sources has been pursued with a realistic TMS model problem. It results that the methods based on surface measurements (schemes 2 and 3) are preferable with respect to the one based on volume measurements (scheme 1). In particular, scheme 1 appears to be sensitive to the choice of the measurement volume unless the number of measurement points is sufficiently large. Moreover, significantly less surface measurements are needed by schemes 2 and 3 to achieve the same accuracy as scheme 1 when noise-free input are provided. It has also been proven that all the schemes are robust when realistic random errors are introduced in the input data. Overall, scheme 3 appears to have the best performance thanks to its intrinsic double regularization and its competitive computational cost.

Despite the considered model problem is a very specific one, the methods discussed in this paper are general. When considering situations in which the dosimetric assessment should be performed on the whole body, like for example TMS effects on the operator instead of the patient [19] or electric fields induced by transformer rooms in workers in their proximity [5], the discrepancy in experimental burden between volume and surface measurements further increases, suggesting the convenience of scheme 3 in many situations.

REFERENCES

[1] L. E. Zaffanella, T. P. Sullivan, and I. Visintainer, "Magnetic Field Characterization of Electrical Appliances as Point Sources through in Situ Measurements," *IEEE Trans. Power Deliv.*, vol. 12, no. 1, pp. 443–449, Jan. 1997.

[2] K. Yamazaki and T. Kawamoto, "Simple Estimation of Equivalent Magnetic Dipole Moment to Characterize ELF Magnetic Fields Generated by Electric Appliances Incorporating Harmonics," *IEEE Trans. Electromagn. C.*, vol. 43, no. 2, pp. 240-244, May 2001.

[3] R. Scorretti, N. Burais, L. Nicolas, and A. Nicolas, "Modeling of Induced Current Into the Human Body by Low-Frequency Magnetic Field From Experimental Data," *IEEE Trans. Magn.*, vol. 41, no. 5, pp. 1992-1995, May 2005.

[4] S. Nishizawa, H.-O. Ruoss, F. M. Landstorfer, and O. Hashimoto, "Numerical Study on an Equivalent Source Model for Inhomogeneous Magnetic Field Dosimetry in the Low-Frequency Range," *IEEE Trans. Biomed. Eng.*, vol. 51, no. 4, pp. 612-616, Apr. 2004.

[5] A. Canova, F. Freschi, M. Repetto, and M. Tartaglia, "Identification of an Equivalent-Source System for Magnetic Stray Field Evaluation," *IEEE Trans. Power Deliv.*, vol. 24, no. 3, pp. 1352-1358, July 2009.

[6] I. Laakso, V. de Santis, S. Cruciani, T. Campi, and M. Feliziani, "Modelling of induced electric fields based on incompletely known magnetic fields," *Phys. Med. Biol.*, vol. 62, pp. 6567-6578, Jul. 2017.

[7] F. Freschi, L. Giaccone, V. Cirimele, and A. Canova, "Numerical assessment of low-frequency dosimetry from sampled magnetic fields," *Phys. Med. Biol.*, vol. 63, art. no. 015029, 2018.

[8] W. Wang, O. Bottauscio, M. Chiampi, D. Giordano, and L. Zilberti, "A procedure to estimate the electric field induced in human body exposed to unknown magnetic sources," *Radiation Protection Dosimetry*, vol. 154, no. 2, pp. 157-163, Apr. 2013.

[9] O. Bottauscio, M. Chiampi, G. Crotti, D. Giordano, W. Wang, and L. Zilberti, "Uncertainty Estimate Associated to the Electric Field Induced inside Human Bodies by Unknown LF Sources," *IEEE Trans. Instrum. and Measur.*, vol. 62, no. 6, pp. 1436-1442, June 2013.

[10] K. H. Madsen, L. Ewald, H. R. Siebner, and A. Thielscher, "Transcranial Magnetic Stimulation: An Automated Procedure to Obtain Coil-specific Models for Field Calculations," *Brain Stimulation*, vol. 8, no. 6, pp. 1205-1208, Nov.-Dec. 2015.

[11] S. Sahoo, "Inverse Vector Operators," arXiv:0804.2239v3, Aug. 2010. Available: https://arxiv.org/abs/0804.2239v3

[12] K.R. Davey and M. Riehl, "Suppressing the Surface Field During Transcranial Magnetic Stimulation," *IEEE Trans. Biomed. Eng.*, vol. 53, no. 2, pp. 190-194, Feb. 2006.

[13] M. Lu and S. Ueno, "Calculating the electric field in real human head by transcranial magnetic stimulation with shield plate," *J. Appl. Phys.*, vol. 105, no. 7, art. no. 07B322, Apr. 2009.

[14] L. Hernandez-Garcia, T. Hall, L. Gomez, and E. Michielssen, "A numerically optimized active shield for improved transcranial magnetic stimulation targeting," *Brain Stimulation*, vol. 3, no. 4, pp. 218–25, Oct. 2010.

[15] L. Gomez, F. Cajko, L. Hernandes-Garcia, A. Grbic, and E. Michielssen, "Numerical Analysis and Design of Single-Source Multicoil TMS for Deep and Focused Brain Stimulation," *IEEE Trans. Biomed. Eng.*, vol. 60, no. 10, pp. 2771-2782, Oct. 2013.

[16] P. Rastogi, E. G. Lee, R. L. Hadimani, and D. C. Jiles, "Transcranial Magnetic Stimulation-coil design with improved focality," *AIP Advances*, vol. 7, no. 5, art. no. 056705, May 2017.

[17] B. Deng, S. Li, B. Li, J. Wang, and Z. Zhang, "Noninvasive Brain Stimulation Using Strong-Coupling Effect of Resonant Magnetics," *IEEE Trans. Magn.*, vol. 53, no. 5, art. no. 5800109, May 2017.

[18] E. F. Karlström, R. Lundström, O. Stensson, and K. H. Mild, "Therapeutic staff exposure to magnetic field pulses during TMS/rTMS treatments," *Bioelectromagnetics*, vol. 27, no. 2, pp. 156–158, Feb. 2006.

[19] O. Bottauscio, M. Zucca, M. Chiampi, and L. Zilberti, "Evaluation of the electric field induced in transcranial magnetic stimulation operators," *IEEE Trans. Magn.*, vol. 52, no. 3, art. no. 5000204, Mar. 2016.

[20] M. Zucca, O. Bottauscio, M. Chiampi, and L. Zilberti, "Operator Safety and Field Focality in Aluminium Shielded Transcranial Magnetic Stimulation," *IEEE Trans. Magn.*,vol. 53, no. 11, Art. no. 5100704, Nov. 2017.

[21] C. M. Collins, B. Yang, Q. X. Yang, and M. B. Smith, "Numerical calculations of the static magnetic field in three-dimensional multi tissue models of the human head," *Magn. Reson. Imag.*, vol. 20, no. 5, pp. 413–424, Jun. 2002.

[22] W. Wang and S. Eisenberg, "A three-dimensional finite element method for computing magnetically induced currents in tissues," *IEEE Trans. Magn.*,vol. 30, no. 6, pp. 5015–23, Nov. 1994.

[23] W. Wang, O. Bottauscio, M. Chiampi, D. Giordano, and L. Zilberti, "An experimental-computational technique for evaluating magnetic field distributions around unknown sources," *IEEE Trans. Magn.*, vol. 49, no. 3, pp. 1143-1148, March 2013.

[24] A. Bossavit, *Computational Electromagnetism*. London, UK: Academic Press, 1998, ch 6.

[25] R. Scorretti, R. V. Sabariego, L. Morel, C. Geuzaine, N. Burais, and L. Nicolas, "Computation of Induced Fields Into the Human Body by Dual Finite Element Formulations," *IEEE Trans. Magn.*, vol. 42, no. 3, pp. 783-786, Feb. 2012.

[26] I. Laakso and A. Hirata, "Fast multigrid-based computation of the induced electric field for transcranial magnetic stimulation.," *Phys. Med. Biol.*, vol. 57, no. 23, pp. 7753–65, Nov. 2012.

[27] A. Quarteroni, R. Sacco, and F. Saleri, *Numerical Mathematics*. New York, NY-US: Springer-Verlag, 2000, ch 4.

[28] P. Alotto, P. Bettini, O. Bottauscio, M. Chiampi, and L. Zilberti, "H-matrix Sparsification Applied to Bioelectromagnetic Analysis of Large Scale Human Models," *IEEE Trans. Magn.*,vol. 53, no. 6, Art. no. 7203504, June 2017.

[29] I. Laakso, S. Tanaka, S. Koyama, V. de Santis, and A. Hirata, "Inter-subject Variability in Electric Fields of Motor Cortical tDCS," *Brain Stimul.*, vol. 8, no. 5, pp. 906-913, Sept.-Oct. 2015.

[30] Joint committee for guides in metrology, JCGM, *Evaluation of Measurement Data—Guide to the expression of uncertainty in measurement*. Paris, France: BIPM, 2008.

[31] G. Marsaglia, "Choosing a point from the surface of a sphere," *Ann. Math. Stat.*, vol. 43, no. 2, pp. 645-646, Apr. 1972.

[32] O. Bottauscio, G. Crotti, S. D'Emilio, G. Farina, and A. Mantini, "Generation of reference electric and magnetic fields for calibration of power-frequency field meters," *IEEE Trans. on Instrum. and Measur.*, vol. 42, no. 2, pp. 547-552, Apr 1993.

Alessandro Arduino received the B.Sc. degree in mathematics for engineering sciences, the M.Sc. degree in mathematical engineering and the Ph.D. degree in electrical, electronics and communications engineering from Politecnico di Torino, Italy, in 2012, 2014, and 2018, respectively.
Since 2018, he is postdoctoral fellow at the Istituto Nazionale di Ricerca Metrologica (INRiM), Torino, Italy. His research interest include mathematical and numerical modelling of electromagnetism applied to biomedical engineering and inverse problems.

Oriano Bottauscio is Research Director at the Istituto Nazionale di Ricerca Metrologica (INRIM), Italy and, since 2015, Head of the Division of Metrology for Quality of Life. He has authored or coauthored more than 200 scientific papers, with around 1700 citations and h-index equal to 20 (source: Scopus).
He is deputy coordinator of the Ph.D. School in Metrology, held by Politecnico di Torino (Italy) in convention with INRIM. From 1996 to 2001, he was a contract Professor at Politecnico di Torino in electrical engineering. His research activity is devoted to computational electromagnetism, with main reference to bioelectromagnetics, electromagnetic dosimetry related to medical equipment, electromagnetic fields and human exposure, and magnetic field mitigation.
He is IEEE Senior Member. He was an Associate Editor (in 2009 and 2011) and Chief Editor (in 2013) of the special issues of the IEEE TRANSACTIONS ON MAGNETICS related to the Soft Magnetic Materials Conference. He was responsible and participated to several national and European research projects. From 2001 to 2005, he was a member of CENELEC TC 106X "Electromagnetic field in human environment"—WG3 "Measurement and calculation procedures in

electric, magnetic and electromagnetic fields (0 Hz–300 GHz)" and from 2002 to 2009 a member of the CIGRE Task Force C4.204 "Magnetic Field Mitigation Techniques." Since 2016, he has been a member of the IEEE TC95, SC6 "EMF Dosimetry Modeling," Working Group 2.

Mario Chiampi received the M.S. degree in electrotechnical engineering from Politecnico di Torino, Italy, in 1973. He was a Research Scientist with the Istituto Elettrotecnico Nazionale Galileo Ferraris, Torino and from 1987 up to 2017 Associated and then Full Professor of fundamentals of electrical engineering with Dipartimento Energia of Politecnico di Torino. He is currently Senior Researcher at Istituto Nazionale di Ricerca Metrologica (INRIM) in Torino.
His research interests include numerical methods for electromagnetics, magnetic material modeling, computer-aided design of electrical devices, and dosimetric analysis of biomedical apparatuses.

Ilkka Laakso (M'14) received the M.Sc.(Tech.) degree in electromagnetics and circuit theory from Helsinki University of Technology, Espoo, Finland, in 2007, and the D.Sc.(Tech.) degree in electromagnetics from Aalto University, Espoo, Finland in 2011.
Between 2013 and 2015, he was a Research Assistant Professor and a Research Associate Professor at the Department of Computer Science and Engineering, Nagoya Institute of Technology. Since 2015, he has been an Assistant Professor in electromagnetics in health technologies at Aalto University. His research interest include computational bioelectromagnetic modeling for assessment of human safety and biomedical applications. He is the author of more than 90 papers published in international journals and conference proceedings.
Dr. Laakso received several awards, including the Ericsson Young Scientist Award, 2011; the Young Scientist Award in URSI Commission B International Symposium on Electromagnetic Theory, Hiroshima, Japan, 2013; and the Young Scientist Award in URSI General Assembly and Scientific Symposium, Montreal, Canada, 2017. He is the secretary of the Subcommittee EMF Dosimetry Modeling of the IEEE International Committee on Electromagnetic Safety and a member of the scientific expert group of the International Commission on Non-ionizing Radiation.

Luca Zilberti received the B.Sc., M.Sc., and Ph.D. degrees in Electrical Engineering from Politecnico di Torino, in 2004, 2006, and 2010, respectively.
Since 2010, he is with the Istituto Nazionale di Ricerca Metrologica, Torino. His research activity is focused on the modeling of electromagnetic phenomena, with particular reference to electromagnetic dosimetry and the biomedical applications of electromagnetic fields.